# Molecular Orientations and True Stress−Strain Relationship in Isotactic Polypropylene Film†

**Yihu Song,‡ Koh-hei Nitta,§ and Norio Nemoto*,‡**

*Department of Molecular and Material Sciences, IGSES, Kyushu University, Hakozaki, Fukuoka 812-8581, Japan, and School of Materials Science, Japan Advanced Institute of Science and Technology, Ishikawa 923-1292, Japan*

*Received March 31, 2003; Revised Manuscript Received July 7, 2003*

ABSTRACT: The microscopic infrared dichroism measurement is made on a quenched iPP thin film during the stepwise elongation to obtain the molecular orientation functions, $f_{am}$ and $f_c$, in the amorphous and the crystalline phases, respectively. Results reveal that the pseudo-affine deformation of the amorphous phase occurs for $f_{am} < 0.45$ with $f_c = 1.85f_{am}$, and concurrent structure alternation of a small portion of crystallites is evidenced from a limited change in the degree of crystallinity $V_c$. The true stress−strain relationship on the mesoscale is discussed on the basis of an interpenetrating network model, in which thin threadlike strands composed of crystallites firmly connected through intercrystalline links (C network) penetrate through an elastic network composed of amorphous chains interconnected to each other with lamellae at cross-linking sites (CEAM network). Combining the Matsuoka viscoelastic constitutive equation and the Takayanagi model for the C network below and above the yielding point, respectively, and the affine deformation equation for the CEAM network, we are allowed to give a straightforward description of the local deformation upon necking.

## Introduction

Particular efforts have been devoted to study the deformation mechanisms of semicrystalline polymers with a special attention to deformation behaviors of the crystalline component with such complicated structures as the individual lamellar crystallite, lamellar stack, and other superstructures like spherulites.[1−14] In uniaxial stretching, intense microshear bands are formed as a sample approaches the yielding point. Further stretching leads to the shear bands to coalesce so as to form a well-shaped neck with two shoulders propagating oppositely at essentially constant nominal stress. It has been argued that the necking on a fine scale is related to the lamellar disintegration[15] or the local melting accompanied by a strain-induced crystallization in the melt phase.[4] The amorphous phase, the counterpart in the semicrystalline polymers, is of importance in determination of the initial modulus and the ultimate properties.[16] Its contribution to deformation is, however, discussed rather ambiguously or almost completely neglected in the literature.[17−19]

The necking is accompanied by a rapid molecular orientation as disclosed from the infrared dichroism.[20−23] In preceding papers,[24,25] we studied deformation behaviors of quenched isotactic polypropylene (iPP) films containing only microcrystallites with equipment constructed for simultaneous kinetic measurements of microscopic infrared (MicIR) dichroism from a predetermined small sampling area and of macroscopic stress of a polymer thin film subjected to uniaxial stretching at a constant low elongation rate. The local deformation is found to be considerably inhomogeneous without any definite relationship with the macroscopic nominal stress−strain behavior.[24] Applying a novel photogrammetry method for in-situ determination of the local strain within the same predetermined sampling area,[25] we found that the area with a mesoscale of 200 × 200 $\mu m^2$ in the film may deform pseudo-affinely during the necking as incompressible material; i.e., the orientation function of the amorphous phase, $f_{am}$, as a function of local draw ratio $\lambda_{Meso}$ agrees with the affine deformation model up to $\lambda_{Meso} \sim 4.5$, while the necking gives rise to unequal shrinkages in the film width and thickness directions.[25] We also found that the orientation function of the crystalline phase, $f_c$, is proportional to $f_{am}$ in the same $\lambda_{Meso}$ region. The latter result has been interpreted as being due to that the microcrystallites or lamellae embedded in the amorphous chain matrix behave as cross-linkers to form an elastic network, and the affine deformation of amorphous iPP chains induces rotation of lamellae during the necking process and results in alignment of the lamellae with the main chain *c* axis parallel to the elongation direction. This network is hereafter called a crystallite-enhanced amorphous matrix (CEAM), and its role in the deformation process of semicrystalline polymers as a whole, especially in the true stress−strain relationship, should be elucidated taking into account earlier results on deformation behaviors of the crystalline component.

The typical value of the Young's modulus calculated from the initial slope of the nominal stress−strain curve was $E = 490$ MPa for our sample. This value is much smaller than $E_c \approx 40$ GPa reported for the modulus exerted by the surface normal to the *c*-axis of the iPP single crystal[26,27] but much larger than the plateau modulus $E_{am} \approx 1.2$ MPa of the entanglement network in melt.[28] A big difference between $E$ and $E_{am}$ inevitably leads to that stress response to a stimulus of imposed continuous stretching must be mainly supported by the crystalline phase which percolates through the whole film and form a network. Application of the Takayanagi model II[29] in which the crystalline and the amorphous phases are aligned in parallel to the stretching direction

† Part IV of Deformation Mechanisms of Polymer Thin Films by Simultaneous Kinetic Measurement of Microscopic Infrared Dichroism and Macroscopic Stress.

‡ Kyushu University.

§ Japan Advanced Institute of Science and Technology.

* To whom correspondence should be addressed. E-mail: nemo@mm.kyushu-u.ac.jp.

10.1021/ma030194d CCC: $25.00 
Published on Web 09/23/2003

allows a rough estimate that the fraction of this crystalline phase is as low as 0.03. Nonetheless, the crystalline phase is plausibly present in the form of elongated molecular aggregates,[30] a part of which is composed of inextensible intercrystalline links connecting adjacent lamellae.[31] This leads to a speculation that there is a possibility for the coexistence of another type of network composed of a crystallites firmly connected through intercrystalline links (C network) with the CEAM network in the iPP film and that cooperative deformations of the two networks, probably interpenetrating to each other, may be considered to occur.

Previous MicIR measurements[25] were performed constantly stretching the iPP film; thus, the process is surely a dynamical one and thermodynamically nonequilibrium, while the affine deformation is applicable, in the strict sense, for the rubberlike network which can almost instantaneously take a new equilibrium conformation in response to applied strain. In semicrystalline polymers, short time local molecular motion is allowed, but global thermal motions in equilibrium are believed to need a very long relaxation time, and furthermore yielding and plastic deformation are closely related to irreversible structural changes in the crystalline phase. Therefore, success of the affine model for description of molecular orientation in the CEAM composite during continuous stretching might be only fortuitous. In this paper, we shall discuss the applicability of the affine model more in detail using data obtained by the stepwise elongation experiment, in which elongation is occasionally stopped and the film is allowed to relax for 3 h, and the same procedures are repeated until a nominal macroscopic draw ratio $\lambda_{Mac}$ reaches 6. We shall also evaluate the true stress−strain relationship in the local sampling area from the data in this work as well as in the previous work,[25] making use of a result that there is no specific volume change observed during elongation and then discuss them on the basis of the interpenetrating network model.

## Experimental Section

**Materials.** The pellets of iPP with $M_w = 3.7 \times 10^5$ were thermally compressed at 210 °C for 5 min to form a film with an average thickness of about 30 $\mu$m, which was then quenched to 0 °C in an ice/water mixture. The as-prepared film was apparently homogeneous and contained microcrystallites of a size less than 10 $\mu$m exclusively.

**Apparatus.** The setup details of the equipment were described elsewhere.[24,32] The sample cell of the elongation device was mounted in the same compartment of FTIR system. The two clamps moved synchronously to the two opposite directions from the film center. The necking forced the original film center where the predetermined sampling area was located to move continuously along the draw $x$-axis. The desired area was adjusted to the viewing field under a microscope at a given time interval of 5 min, moving the $x-y-z$ stage supporting the sample cell.

**Method.** A stepwise elongation experiment was performed to stretch a sample S-I with an initial size of $L_0 \times W_0 \times d_0 =$ 2 mm × 3 mm × 33 $\mu$m (length × width × thickness) at 30.0 ± 0.1 °C with a strain rate $\dot{\epsilon} = 6.3 \times 10^{-3}$ min$^{-1}$ (stretch speed $V_E = 12.6$ $\mu$m min$^{-1}$). During the kinetic measurement, the broad band $AC(t) = A_{\parallel}(t) - A_{\perp}(t)$ and the low pass $DC(t) = A_{\parallel}(t) + A_{\perp}(t)$ signals were alternatively collected from the predetermined sampling area of 200 × 200 $\mu$m$^2$ with a sampling interval of 30 s. Here, $A_{\parallel}(t)$ and $A_{\perp}(t)$ are the polarized spectra with light radiations parallel and perpendicular to the $x$-axis at stretching time $t$, respectively. After elongation was stopped at each $\lambda_{Mac}$ of 1.1, 1.3, 1.6, 2.0, 3.0, 4.0, 5.0, and 6.0, the film was allowed to relax without unloading. During the stress relaxation, the polarized $A_{\parallel}$ and $A_{\perp}$ spectra was measured at selected positions along the $x$-axis using a viewing filed of 50 × 600 $\mu$m$^2$ with the long side vertical to the $x$-axis. It took about 3 h to measure the polarized $A_{\parallel}$ and $A_{\perp}$ spectra at the quiescent state at each $\lambda_{Mac}$.

Another sample S-II with $L_0 \times W_0 \times d_0 = 0.92$ mm × 3 mm × 31 $\mu$m was stretched to $\lambda_{Mac} = 3.0$ and then to $\lambda_{Mac} = 6.4$ with $\dot{\epsilon} = 6.6 \times 10^{-2}$ min$^{-1}$ ($V_E = 60.7$ $\mu$m min$^{-1}$). $A_{\parallel}$ and $A_{\perp}$ spectra were measured along the $x$-axis at the quiescent state.

The MicIR dichroism was evaluated in terms of peak height intensities of the $AC(t)$ and the $DC(t)$ spectra in the kinetic measurement or of the $A_{\parallel}$ and the $A_{\perp}$ spectra in the quiescent measurement. From dichroism of a desired band, the Hermans orientation function $f$ defined by eq 1

$$f = \frac{3\langle \cos^2 \theta \rangle - 1}{2} \tag{1}$$

can be derived through

$$f = \frac{2A(t)}{3 - A(t)} \frac{R_0 + 2}{R_0 - 1} \tag{2}$$

with

$$A(t) = \frac{AC(t)}{DC(t)} \tag{2a}$$

for the kinetic scan and

$$A(t) = \frac{A_{\parallel} - A_{\perp}}{A_{\parallel} + A_{\perp}} \tag{2b}$$

for the rapid scan. Here, $\theta$ is the orientation angle that a chain segment makes with the $x$-axis, and $R_0 = 2 \cot^2 \psi$ is the perfect dichroic ratio of a transition moment, making an angle $\psi$ with the direction of the molecular main chain axis.

$f_c$ and $f_{av}$ were determined from the 998 and 973 cm$^{-1}$ bands, respectively.[33,34] The $\pi$-band at 998 cm$^{-1}$ involves the $CH_3$ rocking, the C−$CH_3$ stretching, the CH bending, and the $CH_2$ twisting modes in the crystalline phase, while the $\pi$-band at 973 cm$^{-1}$ belongs to the $CH_3$ rocking and the axial and equatorial C−C stretching modes in both the amorphous and the crystalline phases.[35] $f_{am}$ was derived on the basis of the two-phase model[33,34] according to

$$f_{av}(t) = V_c f_c(t) + (1 - V_c) f_{am}(t) \tag{3}$$

DSC measurement gave the degree of crystallinity $V_c \approx 0.40$ in two film samples at $\lambda_{Mac} = 1$ and $\lambda_{Mac} = 8$. Small changes in $V_c$ during elongation can be detected from the absorbance ratio $A$(998 cm$^{-1}$)/$A$(973 cm$^{-1}$).[36−39] During deformation, the 973 cm$^{-1}$ band may be used as an internal thickness reference.[36,40,41] Alternatively, we could determine the film thickness in the sampling area from the interference pattern appearing in the polarized or the $DC(t)$ spectra.[32]

The local draw ratio was evaluated from $\lambda_{Meso} = W_0 d_0 / Wd$ and the true stress from $\sigma = \sigma_n \lambda_{Meso}$, since constant specific volume during elongation was satisfied for this film.[25] Here, $W$ and $d$ are the width and the thickness of the sampling area, respectively, at the instant when the stretching is stopped, $W_0$ and $d_0$ values in the undeformed state, and $\sigma_n$ the measured nominal stress.

## Results

**Time Profiles of Stress, Molecular Orientation, and Film Shape.** The time profile of $\sigma_n$ of the film S-I obtained with the stepwise elongation method is shown in Figure 1a, where the variable $t$ on the horizontal axis expresses the total elongation period. Elongation was stopped at eight values of $\lambda_{Mac}$ and, after stopping the film, was allowed to relax for 3 h. The main yielding of

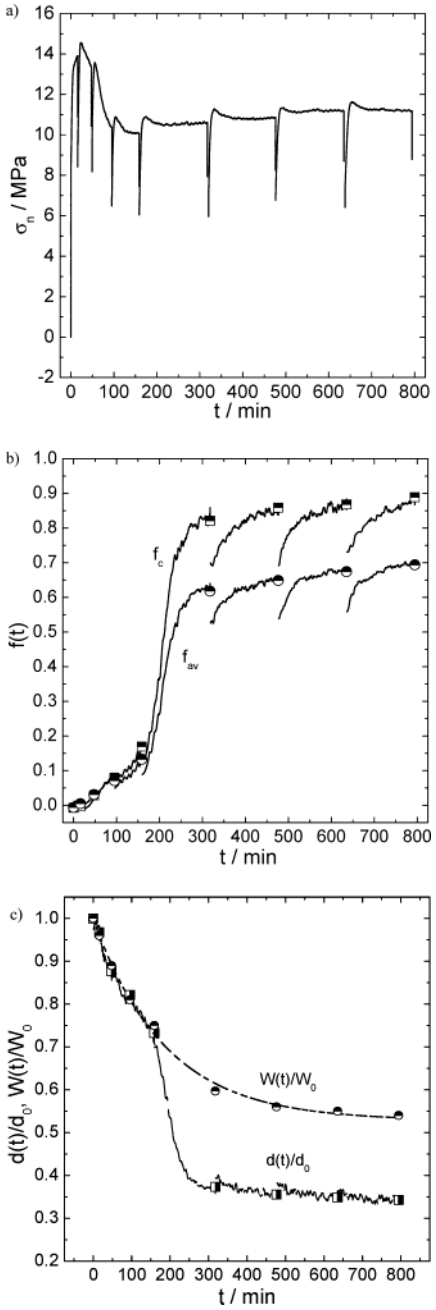


**Figure 1.** Time profiles of nominal stress $\sigma_n$ (a), orientation functions $f_{av}$ and $f_c$ from a sampling area of 200 × 200 $\mu$m$^2$ (b), and relative thickness and width in the sampling area (c) of sample S-I.

the film occurs at $t = 24$ min, whereas subyielding is also observed in restretching the relaxed sample. The stress relaxation data for a time period of 15−20 min after cessation of stretching is also shown in the figure, being characterized by one fast process with a relaxation time of a few minutes along with much slower relaxation processes. This tendency was similar for all stress relaxation data at $\lambda_{Mac}$ measured. Matsuoka[42] has shown that the stress−strain behavior of semicrystalline polymers at small strain before yielding can be described by solving a constitutive equation for the Maxwell model with the modulus $E$ and the relaxation time $\tau_M$ at constant strain rate as

$$\sigma_C = E\epsilon_C\left\{1 - \exp\left(-\frac{\epsilon_{Meso}}{\epsilon_C}\right)\right\} \quad (\epsilon_{Meso} < \epsilon_y) \qquad (4)$$

Here $\epsilon_{Meso} = \lambda_{Meso} - 1$ is local strain, $\epsilon_y$ the yielding strain, and $\epsilon_C = \dot{\epsilon}\tau_M$ a characteristic strain. In inhomogeneous deformation of semicrystalline polymer films at constant elongation rate, initial deformation before yielding occurs uniformly through the whole film, and then severe deformation mainly occurs at the neck shoulders oppositely propagating during stretching, while a portion of the film remains in the initially deformed state. When elongation of the film is stopped, the stress exerted to that portion shall relax with the relaxation time given by eq 4, which may explain the fast relaxation process observed. The latter slow processes are supposed to occur in the neck shoulders and may be related to relaxation of molecular orientation.

Time profiles of $f_c$ and $f_{av}$ sampled from the predetermined sampling area are shown in Figure 1b. Decreases in $f_c$ and $f_{av}$ during stress relaxation are clearly observed, indicating that molecular relaxation indeed occurs for this film. In starting restretching, they gradually increase in contrast to a sharp increase in nominal stress which exhibits a yielding-like phenomena to a small extent once again. $f_c$ and $f_{av}$ are certainly determined by the localized deformation in the close vicinity of the sampling area, but a relation between nominal stress and molecular orientation appears really complicated in this nonequilibrium state.

Figure 1c shows the time dependence of the relative film thickness, $d/d_0$, and the relative width, $W/W_0$, within the sampling area. The latter was measured immediately and 3 h later after stretching of the film was temporarily stopped at prescribed values of $\lambda_{Mac}$, and there was found no change in their values. The film shrinks equally in the thickness ($z$) and width ($y$) directions for $t$ less than 150 min, where molecules are oriented slowly and slightly. From $t = 150$ to 300 min, the shrinkage in thickness is prior to that in width and molecules are oriented dramatically. At $t > 300$ min, the film thickness tends to level off whereas the width decreases continuously. It is to be noted that the thickness $d$ tends to slightly recover during stress relaxation. As long as the sample keeps a property of incompressibility upon deformation, an increase in $d$ gives rise to a decrease in $\lambda$, which is not inconsistent with relaxation of stress as well as molecular orientation functions as illustrated in Figure 1.

Anisotropy in deformation behaviors observed along the width and thickness directions is similar to that found for the same iPP film by continuous elongation and is somewhat comparable with that found in drawing of linear polyethylene (LPE) single-crystal mats.[43] After necking, thickness of a LPE single-crystal mat decreases to less than 5% of the initial value, but the width shrinks very slightly due to anisotropic orientations of the $a$- and $b$-axes.[43] Karacan[44] found that the crystalline chains are more highly oriented than the amorphous chains and tend to orient toward the plane of the film with a strong tendency for the $b$-axis to align normal to the plane of the film. Direct observation by the microscopy on the iPP film reveals that a reduction in $d/d_0$ along the draw axis in the close vicinity of the neck shoulders is much steeper than the corresponding reduction in $W/W_0$. The underlying mechanism remains unclear but might be related to a big difference in macroscopic $W$ and $d$ values of the film tested or to anisotropic shape and associated mechanical strength difference in the iPP lamellae in molecular terms.

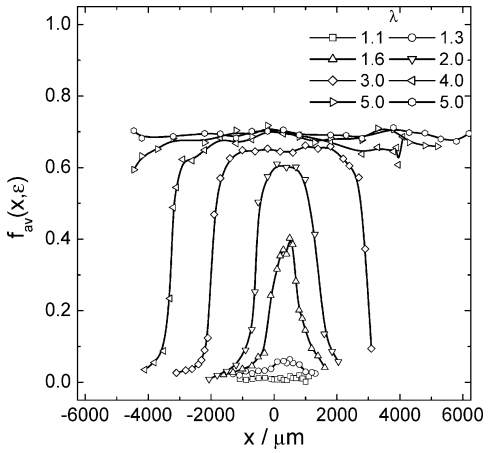


**Figure 2.** A profile of the averaged orientation function $f_{av}$ along the draw $x$-axis of the film S-I at various macroscopic draw ratios $\lambda_{Mac}$.

**Molecular Orientation Gradient at Various $\lambda_{Mac}$.** The profile of the average orientation function $f_{av}$ along the draw ($x$) axis is presented for the film S-I stretched to various $\lambda_{Mac}$ in Figure 2. Although the data were taken during a period of stress relaxation of 3 h, the figure may give a clear image how molecules are going to be oriented due to the neck propagation. $f_{av}(x,\lambda_{Mac})$ shows a very slight molecular orientation near the randomly oriented state in the outer section that has not yet suffered from the necking, an abrupt and sharp orientation gradient along the neck shoulder, and a highly oriented molecular alignment with $f_{av} = 0.6-0.7$ in the necked-down region, namely the neck entity. The necking propagation makes the randomly oriented molecules in the outer section to align the chain axis along the plane of the neck shoulder in the $x$-direction so as to establish an orientation and a deformation gradient. During the propagation of the neck shoulder with such sharp orientation and deformation gradients through a local area, molecules in this area undoubtedly experience a fast transformation from the random to the highly oriented alignment. The orientation gradients in sample S-II were similar to those in S-I, though not shown in the figure.

**Local Crystallinity and Structure Alteration.** Local crystallinity $V_c(t)$ in the sampling area of S-I, estimated from $A_0(998\ cm^{-1})/A_0(973\ cm^{-1})$, is shown in Figure 3 as a function of $t$. It is obvious that a change in $V_c(t)$ is related to two different mechanical processes, i.e., the partial destruction of the original crystallites and the strain-induced crystallization. $V_c(t)$ decreases from 0.40 at $t = 0$ min to 0.38 at $t = 60$ min due to destruction of the original crystallites in passing through the yielding point. The increase in $V_c(t)$ at 60 min $< t <$ 315 min comes from the induced crystallization that seems to overcome the partial destruction. In the neck entity for $t > 315$ min, the two processes might become comparable, resulting in an almost constant $V_c(t)$. A very slight decrease in $V_c(t)$ is observed for $t > 650$ min.

The time dependence of $f_{am}$ reported in the previous papers[24,25] was evaluated from $f_c$ and $f_{av}$ with eq 3 assuming that the crystallinity $V_c$ remained constant upon deformation. Those data were recalculated taking into account a possible 2% decrease in $V_c$ referring to Figure 3 and compared with the $f_{am}$ values obtained by assuming constant $V_c \equiv 0.4$. The correction was found to be negligibly small.

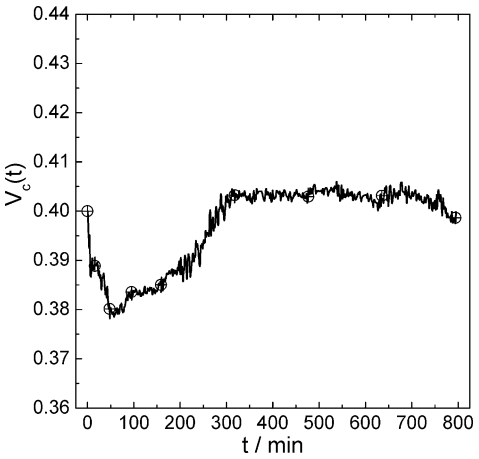


**Figure 3.** Local crystallinity of the sampling area as a function of stretching time $t$.

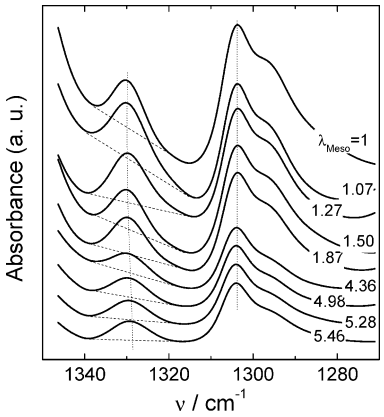


**Figure 4.** Spectra in the 1350−1270 $cm^{-1}$ range sampled from the same sampling area under various local deformations.

The slight change in $V_c(t)$ is involved in structural alternations of both phases. IR absorbance bands at 973, 998, 841, and 1220 $cm^{-1}$ ascribed to absorbance in the crystalline phase do not change their positions and contours upon deformation. We only observe delicate changes in the $\sigma$-band at 1330 $cm^{-1}$ belonging to the $CH_2$ wagging and the CH axial bending modes,[45] as shown in Figure 4. As the local strain increases, this band changes its contour from asymmetrical to symmetrical one accompanied by a decrease in both the wavenumber of peak maximum and the half-peak width. The wavenumber shift of the 1330 $cm^{-1}$ band in our sample is comparable with the finding of Rodríguez-Cabello et al.,[46] who collected Raman spectra simultaneously along with stress−strain data for bulk iPP samples with a spherulitic structure deformed at room temperature. The nonlinear shift of some Raman bands, especially those with high contributions of skeletal vibrations on the applied stress, has been interpreted in terms of the different average orientation accompanying with some degree of backbone chain deformation.

In plotting the peak wavenumber as a function of $\lambda_{Meso}$, we noticed that there are two transition points with the first one at $\lambda_{Meso} = 1.08$ corresponding to the local partial destruction after which the peak position remains constant until $\lambda_{Meso} = 4.36$. At higher strains, the peak maximum is shifted toward low wavenumber rapidly, suggesting the formation of a new structure probably involved in fibrillation.[47−50] Stretching strongly modified the structure of iPP sample in the small restricted region of the neck shoulder. Two different

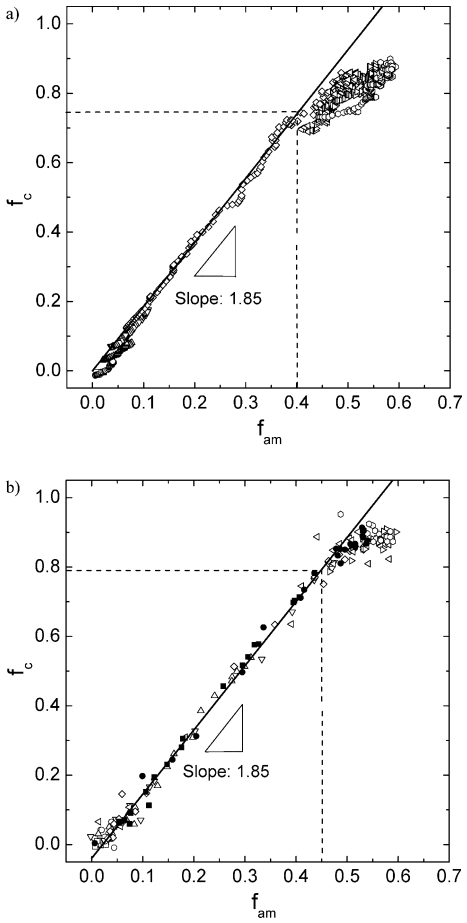


**Figure 5.** Relationship between $f_c$ and $f_{am}$ from the stepwise elongation (a, S-I) and from the quiescent measurement (b, S-I: hollow and S-II: solid).

structures may be coexistent in the transition front, i.e., a newly formed fibrillar structure and the remaining original structure.[49] The small-angle X-ray scattering (SAXS) fiber pattern of a cold-drawn of iPP exhibits only one meridional reflection and continuous scattering on the equator, which suggests that the microparacrystallites are densely packed together laterally into finite extended layers.[51]

Morosoff and Peterlin[52] investigated the wide-angle X-ray scattering (WAXS) pattern of a quenched polypropylene sample drawn at 21 °C as a function of a draw ratio very closely spaced through the neck region. They found that the contribution of the draw ratio to the WAXS pattern of microfibrils could be clearly distinguished from that of deformed spherulites because of the better orientation parallel to the draw direction of the former as compared to the latter. Plastic deformation proceeds through the spherulite deformation accompanied by an increase in chain orientation with strain at small strains or in the outer section. At large strains or in the neck entity, on the other hand, plastic deformation appears to occur exclusively through microfibril formation.

**Relationship between $f_c$ and $f_{am}$.** Figures 5a presents a relationship between $f_c$ and $f_{am}$ calculated using eqs 2, 2a, and 3 from the data shown in Figure 1b. Calculation was also made using eqs 2, 2b, and 3 on the $f_{av}$ data shown in Figure 2 with $f_c$ data from $A(t)$ at 998 $cm^{-1}$ as well as the data obtained for the film S-II, and the results are shown in Figure 5b. The two figures both clearly indicate that $f_c = 1.85 f_{am}$ is valid

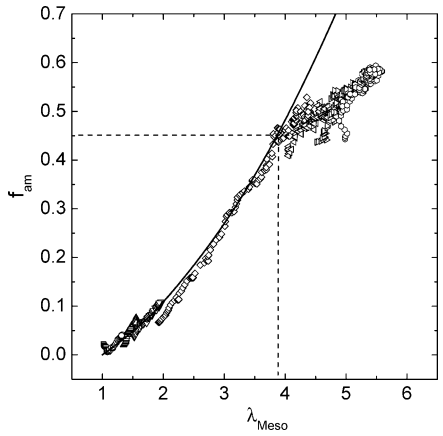


**Figure 6.** A plot of $f_{am}$ against $\lambda_{Meso}$ for the data from the stepwise elongation (S-I).

for $f_{am} \leq 0.40$ or 0.45, which is in excellent agreement with our previous result from continuous elongation of the same iPP film.[25] Thus, we may be allowed to conclude that differences in deformation history do not affect the relationship between $f_c$ and $f_{am}$. For $f_{am} < 0.40$ at least, the lamellar orientation as a function of the amorphous chain deformation obeys the universal law of $f_c = 1.85 f_{am}$ even though the local strain, the local crystallinity, and the contribution of the plastic deformation vary along the neck shoulder from the outer section to the neck entity. At higher $f_{am}$, the increase of $f_c$ may be decelerated as a result of interfibrillar slip, while the considerable scattering of the data in the highly stretched region suggests that multiple processes may take place. In-situ SAXS measurements during elastic and plastic tensile deformation of preoriented samples along the orientation axes by Ginzburg and Tuichiev[53] demonstrated that the microdeformation of highly oriented iPP sample proceeds through two competitive processes of intrafibrillar deformation of long periods and mutual interfibrillar slip. On the other hand, Yamada and Takayanagi[54] found that strain on uniaxial extension of preoriented iPP is related to three processes of crystallite boundary slip ($A_1$), uniform shear deformation of crystallites ($A_2$), and restoration of molecular orientation from the shear deformed state ($A'_2$). Both the $A_1$ and $A_2$ processes predominate before the $A_2-A'_2$ transition, after which the sample is deformed by a molecular process as pulling out the isolated extending chains from the folded chain crystals followed by their refolding.

**Relationship between $f_{am}$ and $\lambda_{Meso}$.** Figure 6 shows a plot of $f_{am}$ against the local draw ratio $\lambda_{Meso}$ in the predetermined sampling area obtained with the stepwise elongation method and is fitted by eq 5, being the prediction of the affine deformation model with an adjustable parameter $N_k$ of the mean number of freely jointed Kuhn segment between cross-links.[55,56]

$$f_{am} = \frac{1}{5N_k}(\lambda_{Meso}^{\ 2} - \lambda_{Meso}^{\ -1}) \qquad (5)$$

The solid curve with $N_k = 6.7$ looks to describe the $\lambda_{Meso}$ dependence of $f_{am}$ up to $f_{am} = 0.45$ ($\lambda_{Meso} = 3.9$), even though there always occurs a small downward deviation presumably as being due to a decrease in $f_{am}$ caused by the long-time stress relaxation. $N_k = 6.7$ is not inconsistent with $N_k = 11$ found in the sample stretched continuously with a larger elongation rate.[25] The limit-

ing value of $f_{am} = 0.45$ below which eq 5 is applicable agrees well with the theoretical prediction $\langle \cos^2 \theta \rangle_{max} \cong 0.6$ for Gaussian network chains fully stretched.[57] In this connection, it should be remarked here that the position of $f_{am} = 0.45$ corresponding to $f_{av} = 0.6$ in Figure 2 is located near the boundary between the neck shoulder and the neck entity. The CEAM network with fully stretched network strands would resist against further deformation, unless the lamellae embedded in the amorphous matrix break. This may partly explain why the neck shoulder appears to smoothly propagate for $\lambda_{Mac} > 2$, while keeping its shape unchanged as illustrated in Figure 2. It is likely that $f_{am} = 0.45$ is a key value to stipulate a limit of the pseudo-affine type of deformation occurring in the narrow neck shoulder region. It seems of natural consequence that for $f_{am} > 0.45$ in the neck entity the molecular orientation becomes slower than the prediction of the affine mode due to breakdown of lamellae behaving as cross-linkers and subsequent localized fibrillation as demonstrated using the other methods.[47−54]

## Discussion

**True Stress−Strain Relationship.** Strobl et al.[58−60] have performed extensive experimental studies on the uniaxial drawing of polyethylene and syndiotactic polypropylene and found a general description for the deformation process. Along a true stress−strain curve, one always distinguishes critical strains related to the onset of isolated slip, a change into a collective activity of slips, fragmentation of the lamellar crystals, and the beginning of fibril formation. They argued that the system is built up by two interpenetrating networks, i.e., the entangled fluid part and the crystallites. When the system is deformed, the crystalline network first supports the applied force. The deformation of the crystalline network forces the entangled melt to follow its shape, which leads to an orientation of the amorphous part. When the deformation is large, the force generated from the entangled amorphous phase may reach a critical value above which the lamellar blocks are no longer stable, and then disintegrated blocks recrystallize along the drawing direction to form fibrils.

The deformation behavior of a molecular network underpinning the semicrystalline morphology was identified as a key factor in the drawing process by Capaccio and Ward.[61] The persistence of a molecular network into the deformed material is strongly supported by shrinkage and shrinkage force measurements.[62] Convincing evidence was also provided by neutron diffraction measurements of the molecular radius of gyration in oriented samples, which suggests that the network deforms affinely.[63]

Our studies in-situ MicIR on molecular orientations in the predetermined local sampling area of the iPP film disclosed three characteristic features that (1) amorphous chains are oriented following the prediction of the pseudo-affine model until they pass through the neck shoulder, (2) molecular orientation in the crystalline phase is described by $f_c = 1.85 f_{am}$ in the same region of local draw ratio $\lambda_{Meso}$, and (3) the neck shoulder ends up when amorphous chains constituting the network reach the fully stretched state characterized by $f_{am} = 0.45$. On the basis of these findings, we proposed the CEAM network in which amorphous chains are interconnected to each other with lamellae at cross-linking sites. If this model is acceptable, the true stress−strain behavior of this network must follow the prediction of the affine model as shown in eq 6.

$$\sigma_{CEAM} = M_{PT}(\lambda_{Meso}^{\ 2} - \lambda_{Meso}^{\ -1}) \tag{6}$$

where $M_{PT}$ is the apparent shear modulus of the network and differs from the conventional meaning of the rubber shear modulus in the Gaussian stress−extension relation.[64] An effect of finite chain length to the amorphous chain and also a filler effect of lamellae in the amorphous matrix are neglected in eq 6 for simplicity, since incorporation of two effects needs an increased number of adjustable parameters.

Equation 4 is useful for dealing with the deformation behavior before yielding but fails to give a physical picture after the yielding and cannot give a correct estimate of stress supported by the C network, $\sigma_c$, at large $\lambda_{Meso}$ beyond the yield point. We here pay particular attention to two papers reported by Vadimsky et al.[31] and Takayanagi and Nitta.[65] The first paper clearly demonstrated that there exist strong and virtually inextensible intercrystalline links which firmly connect adjacent lamellae, lamellar clusters, and spherlulites, whatever they are, in the sample and that, by concentrating applied stress, they commonly induce these lamellae to begin yielding in region close to their points of attachment. In the second paper, the tie molecule model was successfully applied for the postyielding deformation of semicrystalline polymers. This model assumes that a constant number $\nu$ of tie molecules are being pulled out from a lamellar fragment during elongation, and their lengths monotonically increase under a constant force $\nu f_0$ until a critical strain is reached. Here, $f_0$ is the force necessary to draw out a tie molecule from a folded lamellar fragment and is assumed constant during postyielding deformation. In combining these two results of Vadimsky et al.[31] and Takayanagi and Nitta,[65] a small decrease in $V_c(t)$ in the region encompassing the yield point, as is shown in Figure 3, may be interpreted as a result of unfolding of chains in lamellae attached to intercrystalline links, which produces tie molecules extending upon further deformation, resulting in constant exertion of force.

The true stress−strain relationship observed may be simply explained considering an interpenetrating network model, one being the CEAM network and another the C network composed of intercrystalline links and otherwise almost pure crystallites. It seems reasonable to suppose that a considerable number of amorphous chains in the bulky CEAM network adhere at their chain ends to crystallites belonging to the C network, so that close interrelation between deformation behaviors of molecules in the two network may be expected, as revealed by the straightforward relationship $f_c = 1.85 f_{am}$. It may be noted that, in this model, deformation of the C network induces irreversible structural changes in the neck shoulder region and that the force exerted by individual rigid intercrystalline links undergoing the plastic flow is the viscous force; thus, it may depend on the strain rate.

This interpenetrating network model allows us to consider that total stress can be expressed as a sum of contributions from the two networks, since the two networks are simultaneously stretched.

$$\sigma = \sigma_C + \sigma_{CEAM} \tag{7}$$

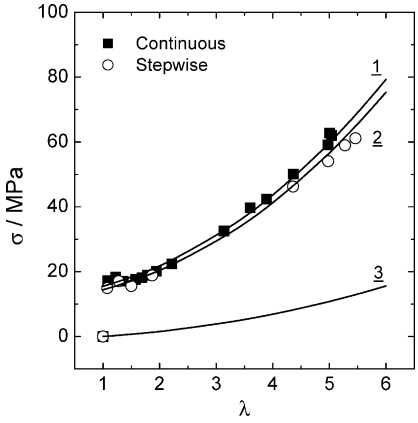


**Figure 7.** True stress $\sigma$ as a function of $\lambda_{Meso}$ for the film S-I measured immediately after the stepwise elongation is stopped (○) and for the previously reported sample[25] measured during continuous deformation (■). Curves 1 and 2 are calculated according to eq 7, and curve 3 gives the theoretical prediction of the affine deformation of the amorphous entanglement network of iPP network according to eq 6.[28]

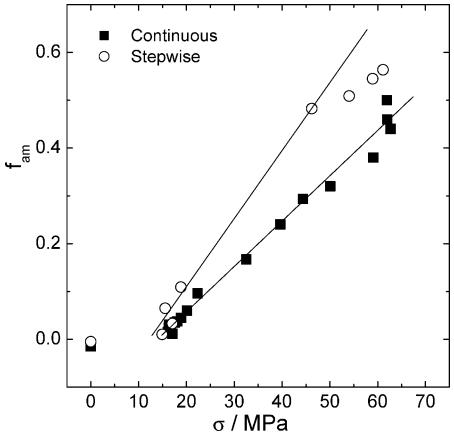


**Figure 8.** Plot of $f_{am}$ against true stress $\sigma$ for the sample S-I measured immediately after the stepwise elongation is stopped (○) and for the previously reported sample[25] measured during continuous deformation (■).

After yielding, deformation of the C network is depicted by the tie molecule model, and the $\sigma_c$ value may be put equal to the observed yield stress $\sigma_y$ to a good approximation immediately after yielding occurred in the neck shoulder. This viscous stress depends on temperature as well as the strain rate. The experiment has been conducted at constant temperature, and an increase in the local draw ratio $\lambda_{Meso}$ with elongation time is very rapid compared to the macroscopic elongation rate applied, as shown in Figure 7 of ref 25, so that its time profile may be approximated as an exponentially increasing function up to $\lambda_{Meso} = 4$, which indicates that the intercrystalline links are flowing at a constant strain rate. Thus, it is likely that $\sigma_c$ takes the constant value of $\sigma_y$ during deformation of the samples in the neck shoulder

$$\sigma_C = \sigma_y \quad (\lambda_{Meso} > \lambda_y) \tag{8}$$

Unfolding of chains from lamellae belonging to the C network induces deformation of the CEAM network whose stress is given by eq 6 and molecular orientation unless the chains are fully stretched; i.e., $f_{am}$ is less than 0.45. It seems pertinent to remark here on a study done by G'Sell and Jonas.[66] They measured true stress−strain curves of seven commercial polymers and proposed that the true stress can be better expressed with an additive equation of two stress components, one being sensitive to strain rate and another to strain. Their equation is essentially same as eq 7.

We estimated the true stress−strain relationship in the local sampling area from the data for the sample S-I obtained immediately after the elongation is stopped as well as those obtained by continuous stretching in the previous work.[25] Results shown in Figure 7 exhibit that $\sigma$ sharply increases at small $\lambda_{Meso}$, which is followed by a monotonic increase with increasing $\lambda_{Meso}$. In the figure, the solid curve 3 is the one calculated for amorphous entanglement network of iPP from eq 6 using the $M_{PT}$ value estimated from the plateau modulus $G_N^0 = 0.435$ MPa.[28] An increase in $\sigma$ with deformation is seen faster for the iPP film. Employing eqs 6−8 with $\sigma_y$ and $M_{PT}$ as adjustable parameters, fitting was made to the two sets of data points satisfying this restriction in Figure 7, and results are shown as the solid curves 1 and 2, respectively. The curve 1 with values of $\sigma_y = 15.5$ MPa and $M_{PT} = 1.78$ MPa well reproduces the data obtained by continuous stretching, while the curve 2 with $\sigma_y$ and $M_{PT}$ as 14.4 and 1.70 MPa determined using five data at lower $\sigma$ appears to fairly reproduces the data by stepwise stretching. $\sigma_y$ values are slightly lower but close to the respective experimental ones. $M_{PT}$ appears to be less affected from the deformation history and is about 4 times larger than that of the entanglement network.

The interpenetrating network model can be also examined from a plot of $f_{am}$ against $\sigma$. Since $f_{am}$ and $\sigma_{CEAM}$ depend on $\lambda_{Meso}$ with the same functional form as given by eqs 5 and 6 and deformation of molecules in the C network affects the $f_{am}$ behavior to a negligibly small extent, additivity of stresses from two networks to total stress requests that $f_{am}$ should be linearly proportional to $\sigma$. The plot given in Figure 8 indicates that this is really satisfied for the data with the continuous elongation method, and the value of $\sigma = 14.5$ MPa at $f_{am} = 0$ is close to $\sigma_y = 15.5$ MPa. There is a considerable data scattering for the data with the stepwise elongation method, but linearity of $f_{am}$ against $\sigma$ seems to be obeyed. Thus, we may be allowed to conclude that the interpenetrating network model can satisfactorily predict not only molecular orientations but also the true stress−strain relationship in the narrow region of the neck shoulder of the iPP film subjected to unixial stretching.

Concerning the above conclusion, the following concluding remarks seem pertinent. The applicability of the interpenetrating network model was examined for the uniaxial deformation data of a polyethylene sample with $M_w = 3.6 \times 10^5$.[67] Although the experimental method for determining the true stress−strain relationship is different from ours, we found that the model was able to describe the deformation up to a draw ratio of 6 with reasonable values for $\sigma_y$ and $M_{PT}$. $M_{PT}$ was found to be considerably higher than the typical value of the plateau shear modulus of the melt.[68] This model, however, does not seem to give any clue for solving the anisotropic deformation phenomena between film thickness and width illustrated in Figure 1c. The model is also valid only in a limited range of the postyielding deformation, and the successive more complicated deformation process in the neck entity surely needs more elaborate analysis.

**Acknowledgment.** This work has been partially supported by the Grant-in-Aid for the Scientific Research from Ministry of Education, Culture, Sports, Science and Technology, Japan (No. 10305070), and one of the authors, Y. Song, is grateful to JSPS for the Grant-in-Aid for JSPS Fellows relating to JSPS Fellowship for Foreign Researchers (No. 12000317). We gratefully acknowledge Dr. M. Takayanagi, Professor Emeritus of Kyushu University, for his profound discussions and helpful suggestions.

## References and Notes

(1) Lu, J.; Ravi-Chandar, K. *Int. J. Solids Struct.* **1999**, *36*, 391.
(2) Ferreiro, V.; Pennec, Y.; Seguela, R.; Coulon, G. *Polymer* **2000**, *41*, 1561.
(3) Li, J. X.; Cheung, W. L.; Chan, C. M. *Polymer* **1999**, *40*, 3641.
(4) Flory, P. J.; Yoon, D. Y. *Nature (London)* **1978**, *272*, 226.
(5) Gent, A. N.; Madan, S. *J. Polym. Sci., Polym. Phys. Ed.* **1989**, *27*, 1529.
(6) Shadrake, L. G.; Guiu, F. *Philos. Mag.* **1976**, *34*, 565.
(7) O'Kane, W. J.; Young, R. J.; Ryan, A. J. *J. Macromol. Sci., Phys.* **1995**, *B34*, 427.
(8) Crist, B.; Fisher, C. J.; Howard, P. R. *Macromolecules* **1989**, *22*, 1709.
(9) Hay, I. L.; Keller, A. *Kolloid Z.* **1965**, *204*, 43.
(10) Krupenkin, T. N.; Taylor, P. L. *Macromol. Theory Simul.* **1998**, *7*, 119.
(11) Moginger, B.; Lutz, C.; Polsak, A.; Muller, U. *Colloid Polym. Sci.* **1991**, *269*, 535.
(12) Oliey, R. H.; Bassett, D. C. *J. Macromol. Sci., Phys.* **1994**, *B33*, 209.
(13) Kasai, N.; Kakudo, M. *J. Polym. Sci.* **1964**, *A2*, 1955.
(14) Palmer, R. P.; Cobblod, A. J. *Makromol. Chem.* **1964**, *74*, 174.
(15) Peterlin, A. *J. Mater. Sci.* **1971**, *8*, 490.
(16) Kennedy, M. A.; Peacock, A. J.; Mandelkern, L. *Macromolecules* **1994**, *27*, 5297.
(17) Dahoun, A.; Aboulfaraj, M.; G'sell, C.; Molinari, A.; Canova, G. R. *Polym. Eng. Sci.* **1995**, *35*, 317.
(18) Lee, B. J.; Argon, A. S.; Parks, D. M.; Ahzi, S.; Bartczak, Z. *Polymer* **1993**, *34*, 3555.
(19) Nikolov, S.; Doghri, I.; Pierard, O.; Zealouk, L.; Goldberg, A. *J. Mech. Phys. Solid* **2002**, *50*, 2275.
(20) Onogi, S.; Asada, T.; Takaki, T. *J. Soc. Mater. Sci. Jpn.* **1967**, *16*, 746.
(21) Mackenzie, M. W. *Advances in Applied Fourier Transformation Infrared Spectroscopy*; John Wiley & Sons: New York, 1988.
(22) Bayer, G.; Hoffmann, W.; Siesler, H. W. *Polymer* **1980**, *21*, 235.
(23) Oderkerk, J.; Groeninckx, G.; Soliman, M. *Macromolecules* **2002**, *35*, 3946.
(24) Song, Y.; Shigematsu, Y.; Nitta, K.-H.; Nemoto, N. *Polym. J.* **2002**, *34*, 584.
(25) Song, Y.; Nitta, K.-H.; Nemoto, N. *Macromolecules* **2003**, *36*, 1955.
(26) Tashiro, K.; Kobayashi, M. *Polymer* **1996**, *37*, 1775.
(27) Tashiro, K.; Kobayashi, M.; Tadokoro, H. *Polym. J.* **1992**, *24*, 899.
(28) Eckstein, A.; Suhm, J.; Friedrich, C.; Maier, R.-D.; Sassmannshausen, J.; Bochmann, M.; Mulhaupt, R. *Macromolecules* **1998**, *31*, 1335.
(29) Takayanagi, M.; Harima, H.; Iwata, Y. *Mem. Fac. Eng., Kyushu Univ.* **1963**, *23* 1.
(30) Hadley, D. W.; Ward, I. M. *Rep. Prog. Phys.* **1975**, *38*, 1143.
(31) Vadimsky, R. G.; Keith, H. D.; Padden, F. J. *J. Polym. Sci.* **1969**, *7*, 1367.
(32) Shigematsu, Y.; Takada, A.; Nemoto, N.; Nitta, K.-H. *Rev. Sci. Instrum.* **2001**, *72*, 3927.
(33) Siesler, H. W. *Adv. Polym. Sci.* **1984**, *65*, 1.
(34) Samuels, R. J. *Makromol. Chem. Suppl.* **1981**, *4*, 241.
(35) Snyder, R. G.; Schachtschneider, J. H. *Spectrochim. Acta* **1964**, *20*, 853.
(36) Quynn, R. G.; Riley, J. L.; Young, D. A.; Noether, H. D. *J. Appl. Polym. Sci.* **1959**, *2*, 166.
(37) Abe, K.; Yanagisawa, K. *J. Polym. Sci.* **1959**, *36*, 539.
(38) Heinen, W. *J. Polym. Sci.* **1959**, *38*, 545.
(39) It is an experimental observation that $A_0$(998 cm$^{-1}$)/$A_0$(973 cm$^{-1}$) is linearly dependent on density $\rho$ of iPP films.[36−38] Writing $A_0$(998 cm$^{-1}$)/$A_0$(973 cm$^{-1}$) = $P\rho + Q$ and $\rho = \rho_c V_c + \rho_{am}(1 - V_c)$, we have $A_0$(998 cm$^{-1}$)/$A_0$(973 cm$^{-1}$) = $(P\rho_{am} + Q) + P(\rho_c - \rho_{am})V_c$ with $\rho_{am}$ and $\rho_c$ densities of the amorphous and the crystalline iPP, respectively. $P$ and $Q$ are constants relative to the isotacticity of iPP and the equipment of FTIR spectrometer used. For the complete amorphous iPP, the 998 cm$^{-1}$ disappears so that $P\rho_{am} + Q = 0$ and $V_c \sim A_0$(998 cm$^{-1}$)/$A_0$(973 cm$^{-1}$).
(40) Luongo, J. P. *J. Appl. Polym. Sci.* **1960**, *3*, 302.
(41) Brader, J. J. *J. Appl. Polym. Sci.* **1960**, *3*, 370.
(42) Matsuoka, S. *Relaxation Phenomena in Polymers*, 2nd ed.; Hanser: New York, 1992; Chapter 3.
(43) Ishikawa, K.; Miyasaka, K.; Maeda, M. *J. Polym. Sci., Part A-2* **1969**, *7*, 2029.
(44) Karacan, I.; Taraiya, A. K.; Bower, D. I.; Ward, I. M. *Polymer* **1993**, *34*, 2691.
(45) Wool, R. P.; Boyd, R. H. *J. Appl. Phys.* **1980**, *51*, 5116.
(46) Rodríguez-Cabello, J. C.; Merino, J. C.; Jawhari, T.; Pastor, J. M. *J. Raman Spectrosc.* **1996**, *27*, 463.
(47) Glenz, W.; Peterlin, A. *J. Macromol. Sci., Phys.* **1970**, *B4*, 473.
(48) Dupuis, J.; Legrand, P.; Seguela, R.; Rietsch, F. *Polymer* **1988**, *29*, 626.
(49) Vittoria, V.; De Candia, F.; Capodanno, V.; Peterlin, A. *J. Polym. Sci., Part B: Polym. Phys.* **1986**, *24*, 1009.
(50) RodríGuez-Cabello, J. C.; Alonso, M.; Merino, J. C.; Pastor, J. M.*J. Appl. Polym. Sci.* **1996**, *60*, 1709.
(51) Rognoni, A. F.; Ferracini, E.; Cackovic, J. L.; Cackovic, H. *J. Polym. Sci., Polym. Phys. Ed.* **1984**, *22*, 485.
(52) Morosoff, N.; Peterlin, A. *J. Polym. Sci., Part A-2: Polym. Phys.* **1972**, *10*, 1237.
(53) Ginzburg, B. M.; Tuichiev, S. H. *J. Macromol. Sci., Phys.* **1992**, *B31*, 291.
(54) Yamada, K. Takayanagi, M. *J. Appl. Polym. Sci.* **1979**, *24*, 781.
(55) Kuhn, W.; Grun, F. *Kolloid Z.* **1942**, *101*, 248.
(56) Treloar, R. L. G. *The Physics of Rubber Elasticity*, 3rd ed; Clarendon Press: Oxford, 1975.
(57) Joe, R. J.; Krigbaum, W. R. *J. Appl. Phys.* **1964**, *35*, 2215.
(58) Hiss, R.; Hobeika, S.; Lynn, C.; Strobl, G. *Macromolecules* **1999**, *32*, 4390.
(59) Hobeika, S.; Men, Y.; Strobl, G. *Macromolecules* **2000**, *33*, 1827.
(60) Men, Y.; Strobl, G. *J. Macromol. Sci., Phys.* **2001**, *B40*, 775.
(61) Capaccio, G.; Ward, I. M. *Nature Phys. Sci.* **1973**, *243*, 143.
(62) Capaccio, G.; Ward, I. M.*Colloid Polym. Sci.* **1982**, *260*, 46.
(63) Sadler, D. M.; Barham, P. J. *Polymer* **1990**, *31*, 36.
(64) James, H. M.; Guth, E. J. *Chem. Phys.* **1943**, *11*, 455.
(65) Takayanagi, M.; Nitta, K.-H. *Macromol. Theory Simul.* **1997**, *6*, 181.
(66) G'Sell, C.; Jonas, J. J. *J. Mater. Sci.* **1981**, *16*, 1956.
(67) Strobl, G. *The Physics of Polymers, Concepts for Understanding Their Structures and Behavior*, 2nd ed.; Springer: Verlag, 1997.
(68) Wood-Adams, P. M.; Dealy, J. M.; deGroot, A. W.; Redwine, O. D. *Macromolecules* **2000**, *33*, 7489.

MA030194D